



1 Channel selection method for hyperspectral
2 atmospheric infrared sounder using AIRS data
3 based on layering

4 Shujie Chang^{1,2,3}, Zheng Sheng^{1,2}, Huadong Du^{1,2}, Wei Ge^{1,2} and
5 Wei Zhang^{1,2}

6 ¹ College of Meteorology and Oceanography, National University of
7 Defense Technology, Nanjing, China

8 ² Collaborative Innovation Center on Forecast and Evaluation of
9 Meteorological Disasters, Nanjing University of Information
10 Science and Technology, Nanjing, China

11 ³ South China Sea Institute for Marine Meteorology, Guangdong
12 Ocean University, Zhanjiang, China

13

14 **Correspondence:** Zheng Sheng (19994035@sina.com)

15

16 **Abstract.** Because a satellite channel's ability to resolve
17 hyperspectral data varies with height, an improved channel selection
18 method is proposed based on information content. An effective
19 channel selection scheme for a hyperspectral atmospheric infrared
20 sounder using AIRS data based on layering is proposed. The results
21 are as follows: (1) Using the improved method, the atmospheric
22 retrievable index is more stable, the value reaching 0.54. The



23 distribution of the temperature weight function is more continuous,
24 more closely approximating that of the actual atmosphere; (2)
25 Statistical inversion comparison experiments show that the accuracy
26 of the retrieval temperature, using the improved channel selection
27 method in this paper, is consistent with that of 1Dvar channel
28 selection. In the near space layer especially, from 10 hPa to 0.02 hPa,
29 the accuracy of the retrieval temperature of our improved channel
30 selection method is evidently improved by about 1 K. In general, the
31 accuracy of the retrieval temperature of ICS is improved. Especially,
32 from 100 hPa to 0.01 hPa, the accuracy of ICS can be improved by
33 more than 11 %; (3) Statistical inversion comparison experiments in
34 four typical regions indicate that ICS in this paper is significantly
35 better than NCS and PCS in different regions and shows latitudinal
36 variations. Especially, from 100 hPa to 0.01 hPa, the accuracy of ICS
37 can be improved by 7% to 13%, which means the ICS method
38 selected in this paper is feasible and shows great promise for
39 applications.

40

41 **1 Introduction**

42 Since the successful launch of the first meteorological satellite,
43 TIROS in the 1960s, satellite detection technology has developed
44 rapidly. Meteorological satellites observe Earth's atmosphere from



45 space and are able to record data from regions which are otherwise
46 difficult to observe. Satellite data greatly enrich the content and
47 range of meteorological observations, and consequently, atmospheric
48 exploration technology and meteorological observations have taken
49 us to a new stage in our understanding of weather systems and
50 related phenomena (Fang, 2014). From the perspective of vertical
51 atmospheric detection, satellite instruments are developing rapidly.
52 In their infancy, the traditional infrared detection instruments for
53 detecting atmospheric temperature and moisture profiles, such as
54 TOVS (Smith et al., 1991) or HIRS in ATOVS (Chahine, 1972; Li et
55 al., 2000; Liu, 2007), usually employed filter spectrometry. Even
56 though such instruments have played an important role in improving
57 weather prediction, it is difficult to continue to build upon
58 improvements in terms of detection accuracy and vertical resolution
59 due to the limitation of low spectral resolution. By using this kind of
60 filter-based spectroscopic detection instrument, therefore, it is
61 difficult to meet today's needs in numerical weather prediction (Eyre
62 et al., 1993). To meet this challenge, a series of plans for the creation
63 of high-spectral resolution atmospheric detection instruments has
64 been executed in the United States and in Europe in recent years:
65 One example is the AIRS (Atmospheric Infrared Sounder) on the
66 Earth Observation System, "Aqua", launched on May 4, 2002 from



67 the United States. AIRS has 2378 spectral channels with subpoint at
68 13 km and a detection height from the ground of up to 65 km
69 (Aumann et al., 2003; Hoffmann and Alexander, 2009; Gong et al.,
70 2011). The United States and Europe, in 2010, also installed the
71 CRIS (Cross-track Infrared Sounder) and the IASI (Inter-Attractive
72 Atmospheric Sounding Interferometer) on polar-orbiting satellites.

73 China also attaches great importance to the development of such
74 advanced detection technologies. In the early 1990s, the National
75 Satellite Meteorological Center began to investigate the principles
76 and techniques of hyperspectral resolution atmospheric detection.
77 China's development of interferometric atmospheric vertical
78 detectors eventually led to the launch of Fengyun No. 3, on May 27,
79 2008, and Fengyun No. 4 on December 11, 2016, both of which
80 were equipped with infrared atmospheric detectors. How best to use
81 the hyperspectral resolution detection data obtained from these
82 instruments, to obtain reliable atmospheric temperature and humidity
83 profiles, is an active area of intense study in atmospheric inversion
84 theory.

85 Due to technical limitations, only a limited number of channels
86 could at first be built into the general satellite detection instrument.
87 In this case, channel selection generally involved controlling the
88 channel weight function by utilizing the spectral response



89 characteristics of the channel (such as the center frequency,
90 bandwidth). With the development of detection technology,
91 increasing numbers of hyperspectral detectors were carried on
92 meteorological satellites. Due to the large number of channels and
93 data supported by such instruments today (such as AIRS with 2378
94 channels and IASI with 8461 channels), it has proven extremely
95 cumbersome to store, transmit, and process such data. Moreover,
96 there is a close correlation between each channel, causing an
97 ill-posedness of the inversion, potentially compromising accuracy of
98 the retrieval product based on hyperspectral resolution data.

99 However, hyperspectral detectors have many channels and
100 provide real-time mode prediction systems with vast quantities of
101 data, which can significantly improve prediction accuracy. But, if all
102 the channels are used to retrieve data, the retrieval time considerably
103 increases. Even more problematic are the glut of information
104 produced, and the unsuitability of the calculations for real-time
105 forecasting. Concurrently, the computer processing power must be
106 large enough to meet the demands of all the channels simultaneously
107 within the forecast time. It is important to select a group of channels
108 that can provide as much information as possible from the thousands
109 of channels' observations to improve the calculation efficiency and
110 retrieval quality.



111 Many researchers have studied the channel selection algorithm.
112 Menke (1984) first chose channels using a data precision matrix
113 method. Aires et al. (1999) made the selection using the Jacobian
114 matrix, which has been widely used since then (Aires et al., 2002;
115 Rabier et al., 2010). Rodgers (2000) indicated that there are two
116 useful quantities in measuring the information provided by the
117 observation data: Shannon information content and degrees of
118 freedom. The concept of information capacity then became widely
119 used in satellite channel selection. In 2007, Xu (2007) compared the
120 Shannon information content with the relative entropy, analyzing the
121 information loss and information redundancy. In 2008, Du et al.
122 (2008) introduced the concept of the atmospheric retrievable index
123 (ARI) as a criterion for channel selection, and in 2010, Wakita et al.
124 (2010) produced a scheme for calculating the information content of
125 the various atmospheric parameters in remote sensing using
126 Bayesian estimation theory. Kuai et al. (2010) analyzed both the
127 Shannon information content and degrees of freedom in channel
128 selection when retrieving CO₂ concentrations using thermal infrared
129 remote sensing and indicated that 40 channels could contain 75% of
130 the information from the total of 1016 channels. Cyril et al. (2003)
131 proposed the optimal sensitivity profile method based on the
132 sensitivity of different atmospheric components. Lupu et al. (2012)



133 used degrees of freedom for signals (DFS) to estimate the amount of
134 information contained in observations in the context of observing
135 system experiments. In addition, the singular value decomposition
136 method has also been widely used for channel selection (Prunet et al.,
137 2010; Zhang et al., 2011; Wang et al., 2014). In 2017, Chang et al.
138 (2017) selected a new set of Infrared Atmospheric Sounding
139 Interferometer (IASI) channels using the channel score index (CSI).
140 Richardson et al. (2018) selected 75 from 853 channels using
141 information content analysis to retrieve the cloud optical depth,
142 cloud properties, and position.

143 Today's main methods for channel selection (such as the data
144 precision matrix method (Menke, 1984), singular value
145 decomposition method (Prunet et al., 2010; Zhang et al., 2011; Wang
146 et al., 2014), and the Jacobi method (Aires et al., 1999; Rabier et al.,
147 2010) use only the weight function to study appropriate numerical
148 methods, the use of which allows sensitive channels to be selected.
149 The above-mentioned studies also take into account the sensitivity of
150 each channel to atmospheric parameters during channel selection,
151 while ignoring factors that impact retrieval results. The accuracy of
152 retrieval results depends not only on the channel weight function but
153 also on the channel noise, background field, and the retrieval
154 algorithm.



155 Currently, information content is often employed in channel
156 selection. During retrieval, this method delivers the largest amount
157 of information for the selected channel combination (Rodgers, 1996;
158 Du et al., 2008; He et al., 2012; Richardson et al., 2018). Although
159 this method has made great breakthroughs in both theory and
160 practice, however, it does not take the sensitivity of different
161 channels at different heights into consideration. This paper uses the
162 atmospheric retrievable index (ARI) as the index, which is based on
163 information content (Du et al., 2008; Richardson et al. 2018).
164 Channel selection is made at different heights, and an effective
165 channel selection scheme is proposed which fully considers various
166 factors, including the influence of different channels on the retrieval
167 results at different heights. This ensures the best accuracy of the
168 retrieval product when using the selected channel. In addition,
169 statistical inversion comparison experiments are used to verify the
170 effectiveness of the method.

171

172 **2 Channel selection indicator and scheme**

173 **2.1 Channel selection indicator**

174 According to the concept of information content, the information
175 content contained in a selected channel of a hyperspectral instrument
176 can be described as H (Rodgers, 1996; Rabier et al., 2010). The final



177 expression of H is:

178

$$H = -\frac{1}{2} \ln |\hat{S} S_a^{-1}|$$

179

$$180 = -\frac{1}{2} \ln |(S_a - S_a K^T (K S_a K^T + S_\varepsilon)^{-1} K S_a) S_a^{-1}|, \quad (1)$$

181

182 where S_a is the error covariance matrix of the background or the
183 estimated value of atmospheric profile, \hat{S} represents the observation
184 error covariance matrix of each hyperspectral detector channel,
185 $\hat{S} = (S_a - S_a K^T (K S_a K^T + S_\varepsilon)^{-1} K S_a)$ denotes the covariance
186 matrix after retrieval by hyperspectral data, K is the weight function
187 matrix, which comes from the selected channel in the hyperspectral
188 data with respect to a specific atmospheric profile parameter.

189 In order to describe the accuracy of the retrieval results visually
190 and quantitatively, the atmospheric retrievable index (ARI), p, (Du et
191 al., 2008) is defined as follows:

192

$$193 p = 1 - \exp\left(\frac{1}{2n} \ln |\hat{S} S_a^{-1}|\right), \quad (2)$$

194

195 where S_a is the error covariance matrix of the background or the
196 estimated value of the atmospheric profile, and \hat{S} represents the
197 observation error covariance matrix of each hyperspectral detector



198 channel. Assuming that before and after retrieval, the ratio of the
199 root mean square error of each element in the atmospheric state
200 vector is 1-p, then $|\hat{S}_a^{-1}| = (1 - p)^{2n}$ is derived. By inverting the
201 equation, the ARI that is p can be obtained in Eq. (2), which
202 indicates the relative portion of the error that is eliminated by
203 retrieval. In fact, before and after retrieval, the ratio of the root mean
204 square error of each element cannot be 1-p. Therefore, p defined by
205 Eq. (1) is actually an overall evaluation of the retrieval result.

206

207 **2.2 Channel selection scheme**

208 The principle of channel selection is to find the optimum channel
209 combination after numbering the channels. This combination will
210 make the information content, H, or the ARI defined in this paper as
211 large as possible, in order to maintain the highest possible accuracy
212 in the retrieval results.

213 Let there be M layers in the vertical direction of the atmosphere
214 and N satellite channels. Selecting n from N channels, there will be
215 C_N^n combinations in each layer, leading C_N^n calculations to get C_N^n
216 kinds of p results. Furthermore, under the maximum one p-value, the
217 corresponding channel combination is used as the optimum channel
218 combination; therefore, the entire atmosphere must be calculated
219 $M \cdot C_N^n$ times. However, the calculation $M \cdot C_N^n$ times will be



220 particularly large, which makes this approach impractical in
 221 calculating p for all possible combinations. Therefore, it is necessary
 222 to design an effective calculation scheme, and such a scheme, i.e., a
 223 channel selection method, using iteration is proposed, called the
 224 “sequential absorption method”. The method’s main function is to
 225 select (“absorb”) channels one by one, taking the channel with the
 226 maximum value of p . Through n iterations, n channels can be
 227 selected as the final channel combination. The steps are as follows:

228 (1) The expression of information content in a single channel:

229 First, we use only one channel for retrieval. A row vector, k , in the
 230 weight function matrix, K , is a weight function corresponding to the
 231 channel. A diagonal element, $s_\varepsilon \frac{\partial^2 \Omega}{\partial v^2}$, in the S_ε matrix is the error
 232 variance in the channel. After observation in this channel, the error
 233 covariance matrix is:

$$234 \hat{S} = S_a - S_a k^T (s_\varepsilon + k S_a k^T)^{-1} k S_a. \quad (3)$$

235 It should be noted that $(s_\varepsilon + k S_a k^T)$ is a single value in Eq. (3),
 236 so Eq. (3) can be converted to:

$$237 \hat{S} = \left(I - \frac{S_a k^T k}{(s_\varepsilon + k S_a k^T)} \right) S_a = \left(I - \frac{(k S_a)^T k}{(s_\varepsilon + k (k S_a)^T)} \right) S_a. \quad (4)$$

238 Substituting Eq. (4) into Eq. (2) gives:

$$239 p = 1 - \exp\left(\frac{1}{2n} \ln\left(\left| I - \frac{(k S_a)^T k}{(s_\varepsilon + k (k S_a)^T)} \right|\right)\right). \quad (5)$$

240



241 (2) Simplification of Eq. (5) p matrix:

242 Since S_a is a positive definite symmetric matrix, it can be
 243 decomposed into $S_a = (S_a^{1/2})^T (S_a^{1/2})$ and $S_\varepsilon = (S_\varepsilon^{1/2})^T (S_\varepsilon^{1/2})$.

244

245 Define $R = S_\varepsilon^{1/2} K S_a^{1/2}$. (6)

246

247 The matrix R can then be regarded as a weight function matrix,
 248 normalized by the observed error and pre-observation error. A row
 249 vector of R, $r = s_\varepsilon^{-1/2} k S_a^{1/2}$, represents the normalized weight
 250 function matrix of a single channel. Substituting r into Eq. (5) gives:

251

$$252 \quad p = 1 - \exp\left(\frac{1}{2n} \ln\left(\left|I - \frac{rr^T}{1+rr^T}\right|\right)\right). \quad (7)$$

253

254 For arbitrary row vectors, a and b, using the matrix property
 255 $\det(I + a^T b) = 1 + ba^T$, the new expression for p is:

256

$$257 \quad p = 1 - \exp\left(\frac{1}{2n} \ln\left(1 - \frac{r^T r}{1 + r^T r}\right)\right)$$

$$258 \quad = 1 - \exp\left(\frac{1}{2n} \ln\left(\frac{1}{1 + r^T r}\right)\right)$$

$$259 \quad = 1 - \exp\left(-\frac{1}{2n} \ln(1 + r^T r)\right). \quad (8)$$

259

260 (3) Iteration in a single layer:



261 First, the iteration in a single layer requires the calculation of R .
262 According to S_a , S_ε , K and Eq. (6), R , which is r corresponding to
263 all the selected channels, can be calculated. Second, using Eq. (8), p
264 of each candidate channel can be calculated. Moreover, the channel
265 corresponding to maximum p is the selected channel for this
266 iteration. After a channel has been selected, according to Eq. (3) we
267 can use \hat{S} to get S_a for the next iteration. Finally, channels which
268 are not selected during this iteration are used as the candidate
269 channels for the next iteration.

270 When selecting n from N channels, it is necessary to calculate
271 $(N-n/2)n \approx Nn$ p values, which is much smaller than C_N^n . Of course,
272 the combination selected by this method is not completely
273 equivalent to the channel combination corresponding to the optimum
274 value of C_N^n p , but it still satisfies the optimum value in a certain
275 sense. In addition to its high computational efficiency by using this
276 method, another advantage is that all channels can be recorded in the
277 order in which they are selected. In the actual application, if n'
278 channels are needed, and $n' < n$, we will not need to select the
279 channel again, but record the selected channel only.

280 (4) Iteration for different altitudes:

281 Because satellite channel sensitivity varies with height, repeating
282 the iterative process of step (3), selects the optimum channels at



283 different heights. Assuming there are M layers in the atmosphere and
284 selecting n from N channels, it is necessary to calculate $M \cdot (N -$
285 $n/2)n \approx M \cdot Nn$ p values, a much smaller number than $M \cdot C_N^n$.

286

287 **2.3 Statistical inversion method**

288 The inversion method of the atmospheric temperature profile can be
289 summarized in two categories: statistical inversion and physical
290 inversion. Statistical inversion is essentially a linear regression
291 model which uses a large number of satellite measurements and
292 atmospheric parameters to match samples and calculate their
293 correlation coefficient. Then, based on the correlation coefficient, the
294 required parameters of the independent measurements obtained by
295 the satellite are retrieved. Because the method does not directly solve
296 the radiation transfer equation, it has the advantages of fast
297 calculation speed. In addition, the solution is stable, which makes it
298 one of the highest precision methods (Chedin et al., 1985). Therefore,
299 the statistical inversion method will be used for our channel
300 selection experiment and a regression equation will be established.

301 According to an empirical orthogonal function, the atmospheric
302 temperature (or humidity), T , and the bright temperature, T_b , are
303 expanded thus:

304



305 $T = T^* \cdot A,$ (9)

306

307 $T_b = T_b^* \cdot A,$ (10)

308

309 where T^* and T_b^* are the eigenvectors of the covariance matrix of
310 temperature (or humidity) and brightness temperature, respectively.

311 A and B stand for the corresponding expansion coefficient vectors of
312 temperature (humidity) and brightness temperature.

313 Using the least squares method and the orthogonal property, the
314 coefficient conversion matrix, V, is introduced:

315

316 $A = V \cdot B,$ (11)

317

318 where $V = AB^T(BB^T)^{-1}.$ (12)

319

320 Using the orthogonality, we get:

321

322 $B = (T_b^*)^T T_b,$ (13)

323

324 $A = (T^*)^T T.$ (14)

325

326 For convenience, the anomalies of the state vector (atmospheric



327 temperature), T , and the observation vector (bright temperature), T_b ,
328 are taken:

329

$$330 \quad \hat{T} = \bar{T} + \hat{T}' = \bar{T} + GT_b' = \bar{T} + G(T_b - \bar{T}_b), \quad (15)$$

331

332 where \bar{T} and \bar{T}_b are the corresponding average values of the
333 elements, respectively. T' and T_b' represent the corresponding
334 anomalies of the elements, respectively.

335 Assuming there are k sets of observations, a sample anomaly
336 matrix with k vectors can be constructed:

337

$$338 \quad T' = (t_1', t_2', \dots, t_k'), \quad (16)$$

339

$$340 \quad T_b' = (t_{b1}', t_{b2}', \dots, t_{bk}'). \quad (17)$$

341

342 Define the inversion error matrix as:

343

$$344 \quad \delta = \bar{T} - \hat{T} = \hat{T}' - T'. \quad (18)$$

345

346 The retrieval error covariance matrix is:

347

$$S_\delta = \frac{1}{k - n - 1} \delta \delta^T$$



$$\begin{aligned}
 348 \quad &= \frac{1}{k-n-1} (T' - GT'_b)(T' - GT'_b)^T \\
 349 \quad &= \frac{k-1}{k-n-1} (S_e - G^T S_{xy} - S_{xy} G^T + GS_y G^T), \quad (19)
 \end{aligned}$$

350

351 where

352

$$\begin{aligned}
 353 \quad S_e &= \frac{1}{k-1} T' T'^T, \\
 354 \quad S_y &= \frac{1}{k-1} T'_b T_b'^T, \\
 355 \quad S_{xy} &= \frac{1}{k-1} T' T_b'^T. \quad (20)
 \end{aligned}$$

356

357 S_e stands for the sample covariance matrix of T , S_y denotes the
 358 sample covariance matrix of T_b , and S_{xy} represents the covariance
 359 matrix of T and T_b . The elements on the diagonal of the error
 360 covariance matrix, S_δ , represent the retrieval error variance of T .

361 The matrix G that minimizes the overall error variance is the least
 362 squares coefficient matrix of the regression equation (15), which
 363 meets the criteria:

364

$$365 \quad \delta^2 = \text{tr}(S_\delta) = \min. \quad (21)$$

366

367 Equation (21) takes a derivative with respect to G , $\frac{\partial}{\partial G} \text{tr}(S_\delta) =$
 368 $0 = (-2S_{xy} + 2GS_y)$, which means that:



369

$$370 \quad G = S_{xy}S_y^{-1}. \quad (22)$$

371

372 Substituting Eq. (22) into Eq. (15) finally gives the least squares
373 solution as:

374

$$375 \quad \hat{T} = \bar{T} + S_{xy}S_y^{-1}(T_b - \bar{T}_b). \quad (23)$$

376

377 It should be noted that the least squares solution obtained here
378 aims to minimize the sum of the error variance for each element in
379 the atmospheric state vector after retrieval of observations has been
380 completed several times. At present, statistical multiple regression is
381 widely used in the retrieval of atmospheric profiles based on
382 atmospheric remote sensing data. As long as there are enough data,
383 S_{xy} and S_y can be determined.

384

385 **3. Channel selection experiment**

386 **3.1 Data and model**

387 The Atmospheric Infrared Sounder (AIRS) instrument suite is
388 designed to measure the Earth's atmospheric water vapor and
389 temperature profiles on a global scale. AIRS is a continuously
390 operating cross-track scanning sounder, consisting of a telescope that



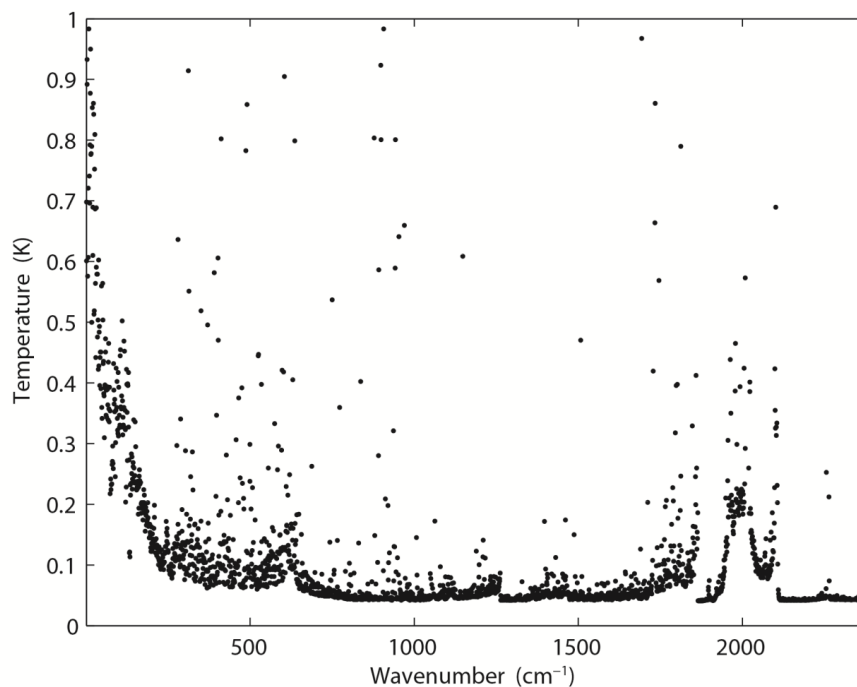
391 feeds an echelle spectrometer. The AIRS infrared spectrometer
392 acquires 2378 spectral samples at a resolution $\lambda/\Delta\lambda$, ranging from
393 1086 to 1570, in three bands: 3.74 μm to 4.61 μm , 6.20 μm to 8.22
394 μm , and 8.8 μm to 15.4 μm . The spatial footprint of the infrared
395 channels is 1.1° in diameter, which corresponds to about 15×15 km
396 at the nadir. The spectral range includes 4.2 μm for important
397 temperature detection, 15 μm for CO_2 , 6.3 μm for water vapor, and
398 9.6 μm for ozone absorption bands. The absolute accuracy of the
399 measured radiation is better than 0.2 K. Moreover, global
400 atmospheric profiles can be detected every day, and the four imaging
401 channels of visible/near infrared are always filled. Due to radiometer
402 noise and faults, there are currently only 2047 effective channels.
403 However, compared with previous infrared detectors, AIRS boasts a
404 significant improvement in both the number of channels and spectral
405 resolution (Aumann, 1994; Huang et al., 2005; Li et al., 2005).

406 AIRS provides real-time mode prediction systems with vast
407 quantities of data, which greatly improves prediction accuracy.
408 However, if all the channels are used to retrieve data, the retrieval
409 time becomes greatly extended. Even more problematic are the huge
410 amounts of information and calculations not being suitable for
411 real-time forecasting.

412 The root mean square error of an AIRS infrared channel is shown



413 in Fig. 1, with black spots, indicating that not all the instrument
414 channels possess a measurement error of less than 0.2 K. There are a
415 few with extremely large measurement errors, which reduce the
416 accuracy of prediction to some extent. Moreover, not all channels
417 possess the same measurement error. At present, more than 300
418 channels have not been used because their errors exceed 1 K. If data
419 from these channels were to be used for retrieval, the accuracy of the
420 retrieval could be reduced. Therefore, it is necessary to select a
421 group of channels to improve the calculation efficiency and retrieval
422 quality. In this paper we study channel selection for temperature
423 profile retrieval by AIRS.



424

425 **Figure 1.** Root mean square error of AIRS infrared channel (black



426 spots).

427

428 For the radiative transfer model and its weight function matrix, K ,
429 the RTTOV v12 fast radiative transfer model is used. RTTOV is an
430 evolution of RTTOV v11, adding and upgrading many features. The
431 model allows rapid simulations (1 ms for 40 channel ATOVS on a
432 desktop PC) of radiances for satellite visible, infrared, or microwave
433 nadir scanning radiometers given atmospheric profiles of
434 temperature and variable gas concentration, and cloud and surface
435 properties. The only mandatory gas included as a variable for
436 RTTOV v12 is water vapor. Optionally, ozone, carbon dioxide,
437 nitrous oxide, methane, carbon monoxide, and sulfur dioxide can be
438 included, with all other constituents assumed to be constant. RTTOV
439 v12 can accept input profiles on any defined set of pressure levels.
440 The majority of RTTOV v12 coefficient files are based on the 54
441 levels shown in Table 1, ranking from 1050 hPa to 0.01 hPa, though
442 coefficients for some hyperspectral sounders are also available on
443 101 levels.

444

445 **Table 1.** Pressure levels adopted for RTTOV v12 54 pressure level
446 coefficients and profile limits within which the transmittance
447 calculations are valid. Note that the gas units here are ppmv.



448 (From <https://www.nwpsaf.eu/site/software/rttov/>, RTTOV Users
 449 guide, 2019).

Level	Pressure	Tmax	Tmin	Qmax	Qmin	Q ₂ max	Q ₂ min	Q ₂ Ref
Number	hPa	K	K	ppmv*	ppmv*	ppmv*	ppmv*	ppmv*
1	0.01	245.95	143.66	5.24	0.91	1.404	0.014	0.296
2	0.01	252.13	154.19	6.03	1.08	1.410	0.069	0.321
3	0.03	263.71	168.42	7.42	1.35	1.496	0.108	0.361
4	0.03	280.12	180.18	8.10	1.58	1.670	0.171	0.527
5	0.13	299.05	194.48	8.44	1.80	2.064	0.228	0.769
6	0.23	318.64	206.21	8.59	1.99	2.365	0.355	1.074
7	0.41	336.24	205.66	8.58	2.49	2.718	0.553	1.471
8	0.67	342.08	197.17	8.34	3.01	3.565	0.731	1.991
9	1.08	340.84	189.50	8.07	3.30	5.333	0.716	2.787
10	1.67	334.68	179.27	7.89	3.20	7.314	0.643	3.756
11	2.50	322.5	17627	7.75	2.92	9.191	0.504	4.864
12	3.65	312.51	175.04	7.69	2.83	10.447	0.745	5.953
13	5.19	303.89	173.07	7.58	2.70	12.336	1.586	6.763
14	7.22	295.48	168.38	7.53	2.54	12.936	1.879	7.109
15	9.84	293.33	166.30	7.36	2.46	12.744	1.322	7.060
16	13.17	287.05	16347	7.20	2.42	11.960	0.719	6.574
17	17.33	283.36	161.49	6.96	2.20	11.105	0.428	5.687
18	22.46	280.93	161.47	6.75	1.71	9.796	0.278	4.705
19	28.69	282.67	162.09	6.46	1.52	8.736	0.164	3.870
20	36.17	27993	162.49	6.14	1.31	7.374	0.107	3.111
21	45.04	27315	164.66	5.90	1.36	6.799	0.055	2.478
22	55.44	265.93	166.19	6.21	1.30	5.710	0.048	1.907
23	67.51	264.7	167.42	9.17	1.16	4.786	0.043	1.440
24	81.37	261.95	159.98	17.89	0.36	4.390	0.038	1.020
25	97.15	262.43	163.95	20.30	0.01	3.619	0.016	0.733



26	114.94	259.57	168.59	33.56	0.01	2.977	0.016	0.604
27	134.83	259.26	169.71	102.24	0.01	2.665	0.016	0.489
28	156.88	260.13	169.42	285.00	0.01	2.351	0.013	0.388
29	181.14	262.27	17063	714.60	0.01	1.973	0.010	0.284
30	207.61	264.45	174.11	1464.00	0.01	1.481	0.013	0.196
31	236.28	270.09	177.12	2475.60	0.01	1.075	0.016	0.145
32	267.10	277.93	181.98	4381.20	0.01	0.774	0.015	0.110
33	300.00	285.18	184.76	6631.20	0.01	0.628	0.015	0.086
34	334.86	293.68	187.69	9450.00	1.29	0.550	0.016	0.073
35	371.55	300.12	190.34	12432.00	1.52	0.447	0.015	0.063
36	409.89	302.63	194.40	15468.00	2.12	0.361	0.015	0.057
37	449.67	304.43	198.46	18564.00	2.36	0.284	0.015	0.054
38	490.85	307.2	201.53	21684.00	2.91	0.247	0.015	0.052
39	532.56	31217	202.74	24696.00	3.67	0.199	0.015	0.050
40	572.15	31556	201.61	27480.00	3.81	0.191	0.012	0.050
41	618.07	318.26	189.95	30288.00	6.82	0.171	0.010	0.049
42	661.00	321.71	189.95	32796.00	6.07	0.128	0.009	0.048
43	703.59	327.95	189.95	55328.00	6.73	0.124	0.009	0.047
44	745.48	333.77	189.95	37692.00	8.71	0.117	0.009	0.046
45	786.33	336.46	189.95	39984.00	8.26	0.115	0.008	0.045
46	825.75	338.54	189.95	42192.00	7.87	0.113	0.008	0.043
47	863.40	342.55	189.95	44220.00	7.53	0.111	0.007	0.041
48	898.93	346.23	189.95	46272.00	7.23	0.108	0.006	0.040
49	931.99	34924	189.95	47736.00	6.97	0.102	0.006	0.038
50	962.26	349.92	189.95	51264.00	6.75	0.099	0.006	0.034
51	989.45	350.09	189.95	49716.00	6.57	0.099	0.006	0.030
52	1013.29	360.09	189.95	47208.00	6.41	0.094	0.006	0.028
53	1033.54	350.09	189.95	47806.00	6.29	0.094	0.006	0.027
54	1050.00	350.09	189.95	47640.00	6.19	0.094	0.006	0.027



451 The weight function matrix, K (Jacobian matrix), in this paper is
452 the weight function matrix of the atmospheric characteristics. In
453 order to correspond to the selected profiles, the atmosphere is
454 divided into 137 layers, each of which contains corresponding
455 atmospheric characteristics, such as temperature, pressure, and the
456 humidity distribution. Each element in the weight function matrix
457 can be written as $\partial y_i / \partial x_j$. The subscript i is used to identify the
458 satellite channel, and the subscript j is used to identify the
459 atmospheric characteristics. Therefore, $\partial y_i / \partial x_j$ indicates the variation
460 in radiation brightness temperature in a given satellite channel, when
461 a given atmospheric characteristic in a given layer changes. We are
462 thus able to establish which layer of the satellite channel is
463 particularly sensitive to which atmospheric characteristic
464 (temperature, various gas contents) in the vertical atmosphere. The
465 RTTOV_K (the K mode), is used to calculate the matrix $H(X_0)$ for a
466 given atmospheric profile characteristic.

467

468 **3.2 Channel selection comparison experiment and results**

469 In order to verify the effectiveness of the method, three sets of
470 comparison experiments were conducted. First, 324 channels used
471 by the EUMETSAT Satellite Application Facility on Numerical
472 Weather Prediction (NWP SAF) were selected. NCS is short for



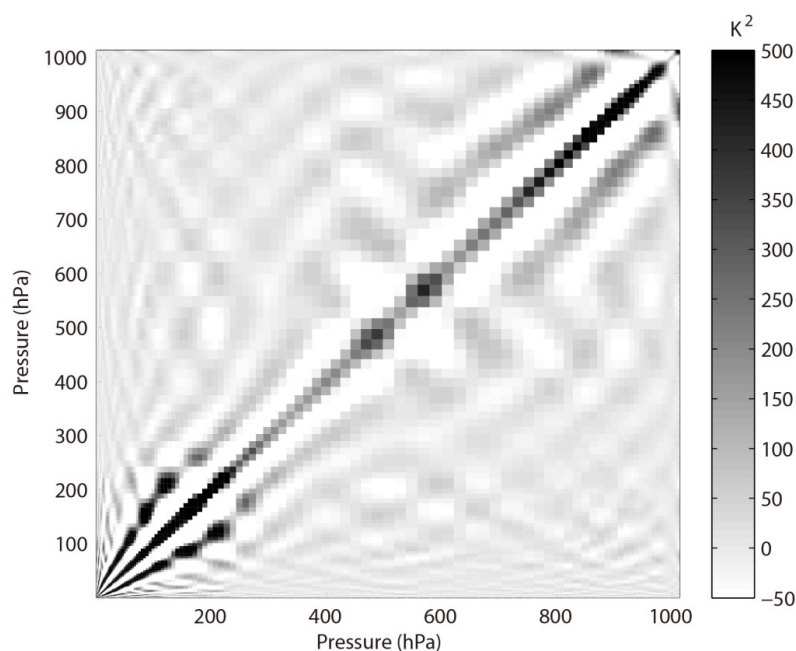
473 NWP channel selection in this paper. The products were released by
474 the NWPSAF 1DVar (one-dimensional variational analysis) scheme,
475 in accordance with the requirements of the NWPSAF. Second, 324
476 channels were selected using the information capacity method. This
477 method was adopted by Du et al. (2008) without the consideration of
478 layering. PCS is short for primary channel selection in this paper.

479 Third, $324 \times M$ channels were selected using the information
480 capacity method for the M layer atmosphere. ICS is short for
481 improved channel selection in this paper. In order to verify the
482 retrieval effectiveness after channel selection, statistical inversion
483 comparison experiments were performed using 5000 temperature
484 profiles provided by the ECMWF dataset, which will be introduced
485 in Sect. 4.

486 The observation error covariance matrix, S_{ϵ} , in the experiment is
487 provided by NWP SAF 1Dvar. In general, it can be converted to a
488 diagonal matrix, the elements of which are the observation error
489 standard deviation of each hyperspectral detector channel, which is
490 the square of the root mean square error for each channel. The root
491 mean square error of an AIRS infrared channel is shown in Fig. 1.
492 The error covariance matrix of the background, S_a , is calculated
493 using 5000 samples of the IFS-137 data provided by the ECMWF
494 dataset (download address:



495 <https://www.nwpsaf.eu/site/update-137-level-nwp-profile-dataset/>,
496 2019). The covariance matrix of temperature is shown in Fig. 2, the
497 results are consistent with the previous study by Du et al. (2008).
498



499
500 **Figure 2.** Error covariance matrix of temperature (shaded).

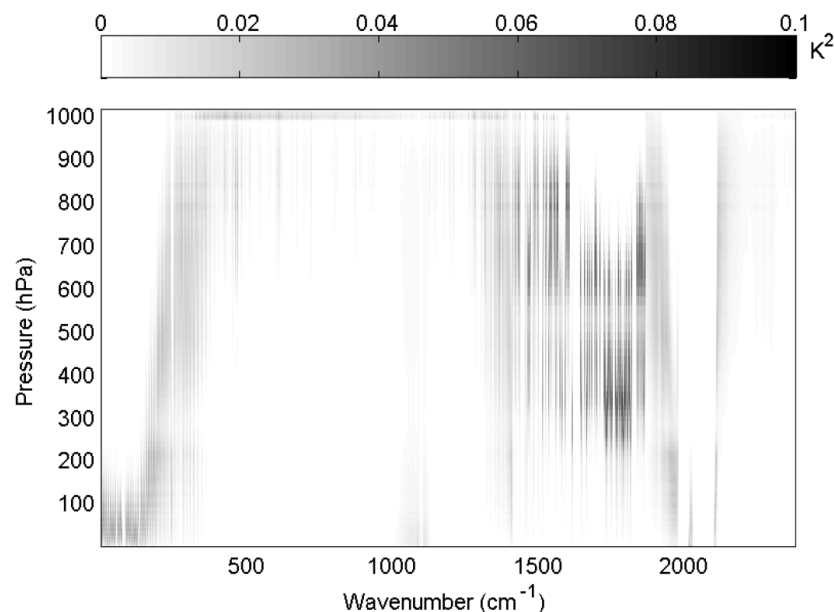
501

502 The reference atmospheric profiles are from the IFS-137 database,
503 and the temperature weight function matrix is calculated using the
504 RTTOV_K mode, as shown in Fig. 3; the results are consistent with
505 those of the previous study by Du et al. (2008). For the air-based
506 passive atmospheric remote sensing studied in this paper, when the
507 same channel detects the atmosphere from different observation



508 angles, the value of the weight function matrix K changes due to the
509 limb effect. Therefore, when we select channels, the results differ
510 because of the different observation angles. But due to the selection
511 principle and method are exactly the same and our key is the
512 selection method; we do not discuss, therefore, the variation in
513 observation angle when making a selection.

514



515

516 **Figure 3.** Temperature weight function matrix (shaded).

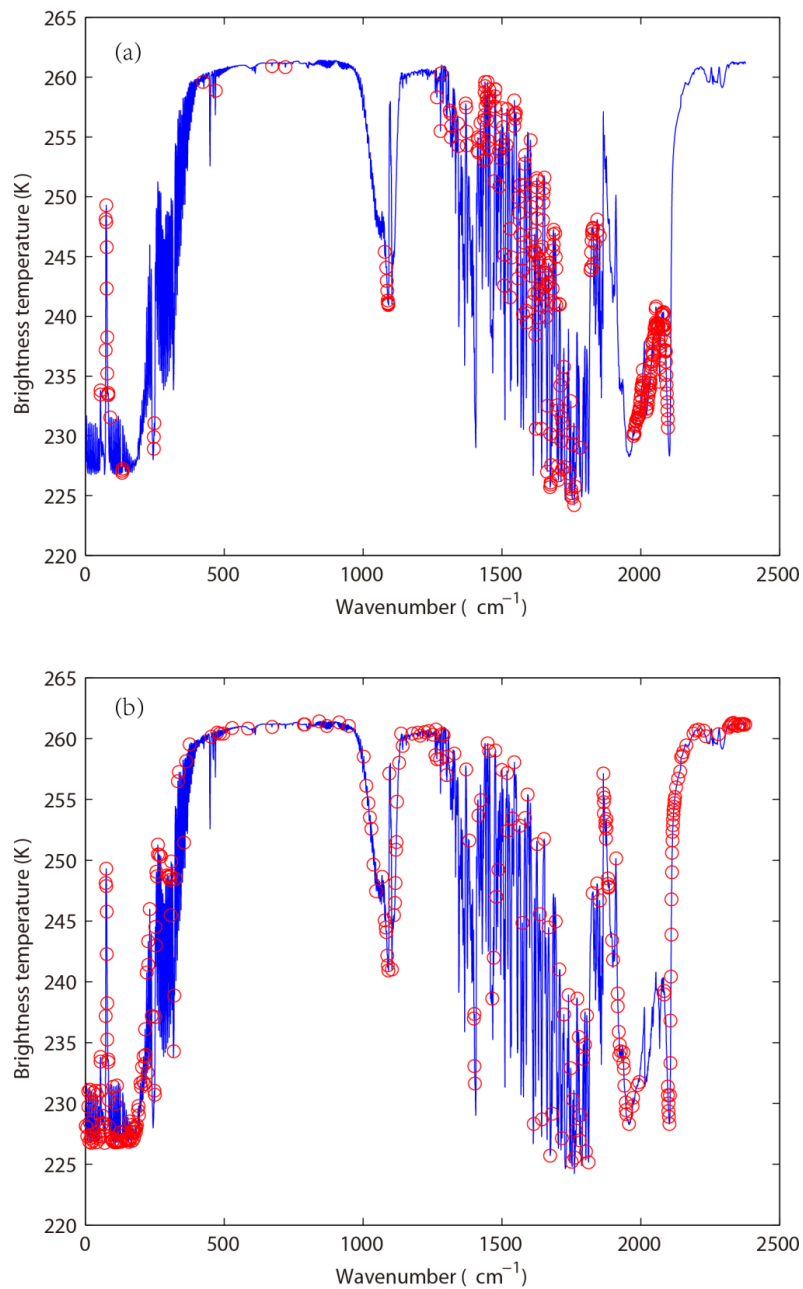
517

518 In order to verify the effectiveness of ICS, the distribution of 324
519 channels, without considering layering, in the AIRS bright
520 temperature spectrum is indicated in Fig. 4. The background



521 brightness temperature is the simulated AIRS observation brightness
522 temperature, which is from the atmospheric profile in RTTOV put
523 into the model. Figure 4(a) shows the 324 channels selected by PCS,
524 while Fig. 4(b) shows the 324 channels selected by NCS.

525



526

527 **Figure 4.** The distribution of different channel selection methods

528 without considering layering in the AIRS bright temperature



529 spectrum (blue line). (a) 324 channels selected by PCS (red circles).
530 (b) 324 channels selected by NCS (red circles).

531 Without considering layering, the main differences between the
532 324 channels selected by PCS and NCS are as follows: (1) When the
533 wavenumber approaches 1000, the wavelength is 11 μm (1/1000).
534 Near this band, fewer channels are selected by PCS because the
535 retrieval of ground temperature is considered by NCS; (2) When the
536 wavenumber is near 1200, the wavelength is 9 μm (1/1200). Near
537 this band, no channels are selected by PCS because the retrieval of
538 O_3 is not considered in this paper; (3) When the wavenumber
539 approaches 1500, the wavelength is 6.7 μm (1/1500). As is known,
540 the spectral range from 6 μm to 7 μm corresponds to water vapor
541 absorption bands, but fewer channels are selected by NCS; (4) When
542 the wavenumber is close to 2000, it derives a wavelength of 5 μm
543 (1/2000), which includes 4.2 μm for N_2O and 4.3 μm for CO_2
544 absorption bands. As is shown in Fig. 4, fewer channels are selected
545 by PCS in those bands. PCS is favorable for atmospheric
546 temperature detection in the high temperature zone; (5) In the near
547 infrared area, the wavenumber exceeds 2200, deriving a wavelength
548 of less than 4 μm (1/2000). A small number of channels is selected
549 by NCS, but no channels are selected by PCS.

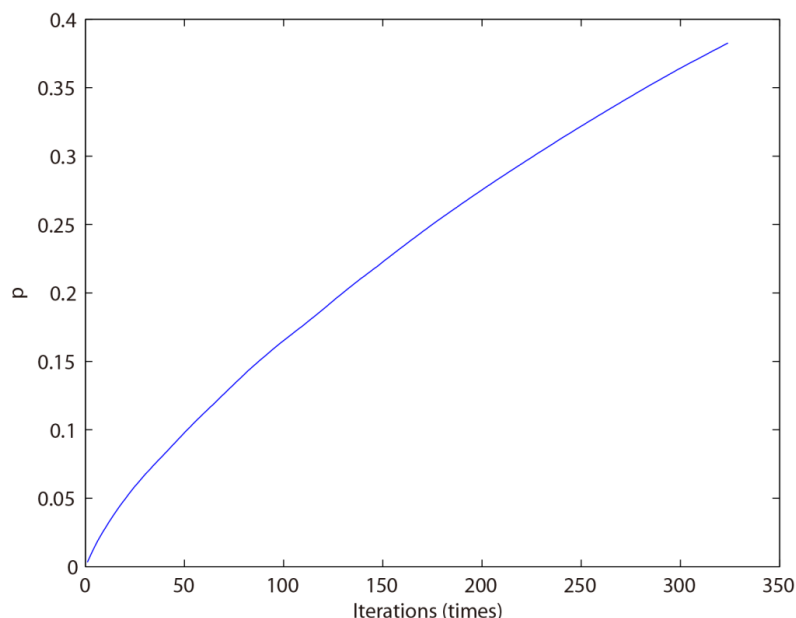
550 Above all, the information content used in this paper only takes



551 the temperature profile retrieval into consideration, so the channel
552 combination of PCS is inferior to that of NCS for the retrieval of
553 surface temperature and the O₃ profile. The advantages of the
554 channel selection method based on information content in this paper
555 are mainly reflected in: (1) Near space (20–100 km) is less affected
556 by the ground surface, so the retrieval result of PCS is better than
557 that of NCS. (2) Due to the method selected in this paper there are
558 more channels at 4.2 μm for N₂O and 4.3 μm for CO₂ absorption
559 bands; the channel combination of PCS is superior to that of NCS
560 for atmospheric temperature detection in the high temperature zone.

561 By comparing channel selection without considering layering,
562 we note the general advantages and disadvantages of PCS and NCS
563 for the retrieval of atmosphere and can improve the channel
564 selection scheme. First, the retrieval of the temperature profile for
565 324 channels selected by PCS is obtained. The relationship between
566 the number of iterations and the ARI is shown in Fig. 5.

567



568

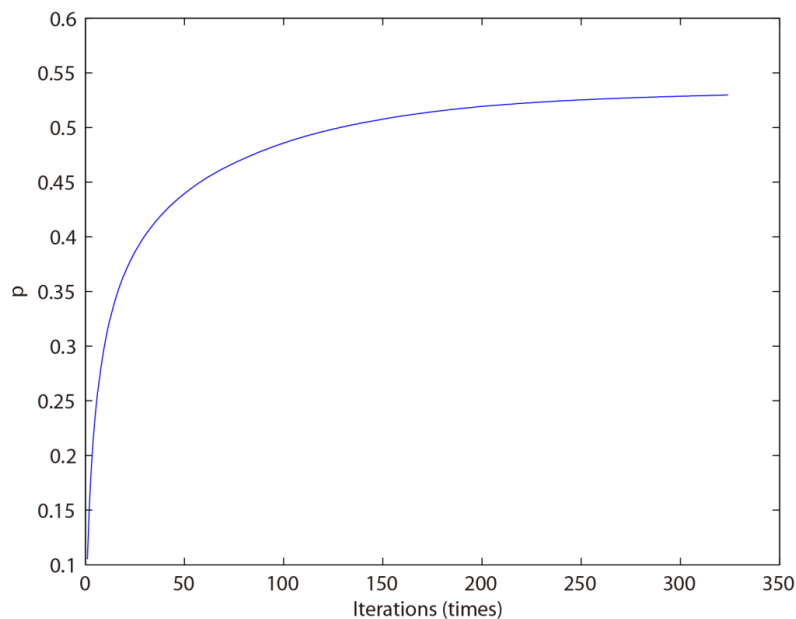
569 **Figure 5.** The relationship between the number of iterations and ARI
570 for PCS.

571

572 The ARI tends to be 0.38 and is not convergent, so the PCS
573 method needs to be improved. In this paper, the atmosphere is
574 divided into 137 layers, and based on the information content and
575 iteration, 324 channels are selected for each layer. Moreover, the
576 temperature profile of each layer can be retrieved. The relationship
577 between the number of iterations and the ARI is shown in Fig. 6.
578 When the number of iterations approaches 100, the ARI of ICS tends
579 to be stable, reaching 0.54. Thus, in terms of the ARI and
580 convergence, the ICS method is superior to that of PCS.



581

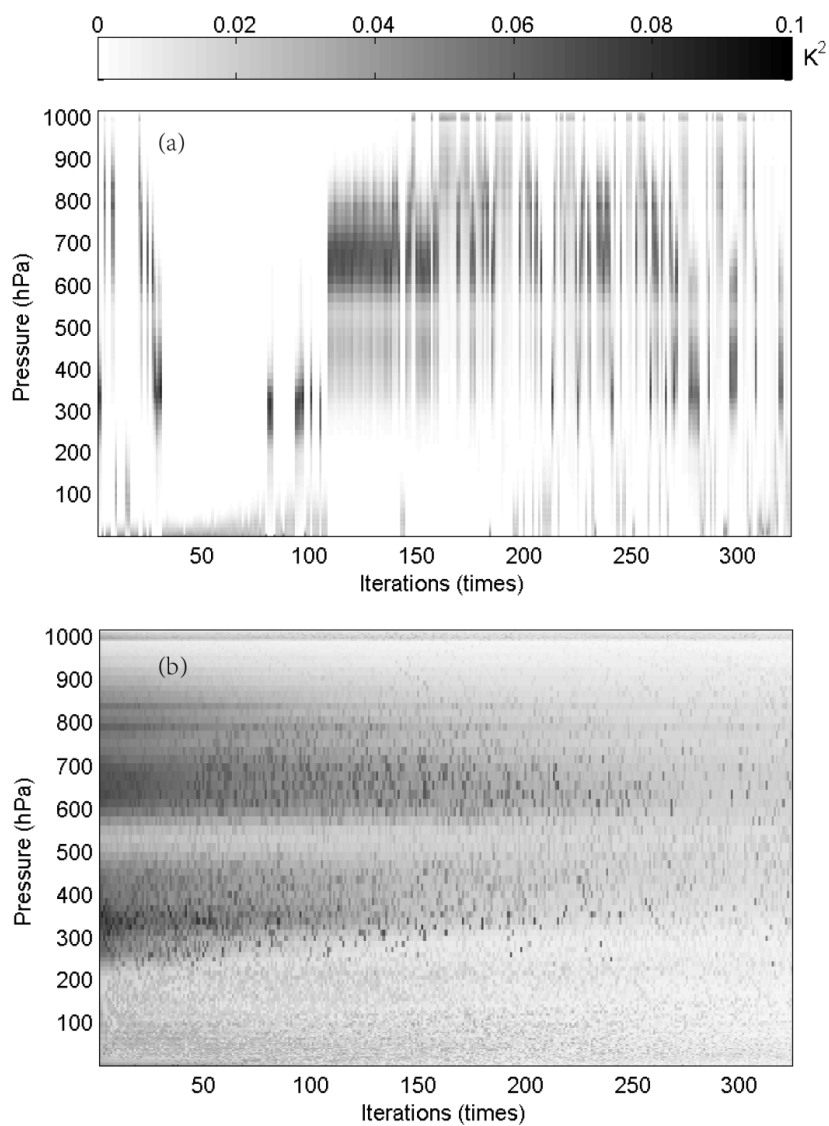


582

583 **Figure 6.** The relationship between the number of iterations and the
584 ARI for ICS.

585

586 Furthermore, because an iterative method is used to select
587 channels, the order of each selected channel is determined by the
588 contribution from the ARI. The weight function matrix of the top
589 324 selected channels, according to channel order, is shown in Fig.
590 7.



591

592 **Figure 7.** The relationship between the number of iterations and the
593 weight function of the top 324 selected channels (shaded). (a) PCS.

594 (b) ICS.

595



596 As illustrated in Fig. 7, in the first 100 iterations, the distribution
597 of the temperature weight function for PCS is relatively scattered; it
598 does not reflect continuity between the adjacent layers of the
599 atmosphere. Besides, the ICS result is better than that of PCS,
600 showing that: (1) the distribution of the temperature weight function
601 is more continuous and reflects the continuity between adjacent
602 layers of the atmosphere; (2) regardless of the number of iterations,
603 the maximum value of the weight function is stable near 300–400
604 hPa and 600–700 hPa, without scattering, which resembles more
605 closely the scenario in real atmosphere.

606

607 **4. Statistical multiple regression experiment**

608 **4.1 Temperature profile database**

609 A new database including a representative collection of 25,000
610 atmospheric profiles from the European Centre for Medium-range
611 Weather Forecasts (ECMWF) was used. The profiles were given in a
612 137-level vertical grid extending from the surface up to 0.01 hPa.
613 The database was divided into five subsets focusing on diverse
614 sampling characteristics such as temperature, specific humidity,
615 ozone mixing ratio, cloud condensates, and precipitation. In contrast
616 with earlier releases of the ECMWF diverse profile database, the
617 137-level database places greater emphasis on preserving the



618 statistical properties of sampled distributions produced by the
 619 Integrated Forecasting System (IFS). IFS-137 spans the period from
 620 September 1, 2013 to August 31, 2014. There are two operational
 621 analyses each day (at 00z and 12z), and the modeling grid contains
 622 2,140,702 grid points. The pressure levels adopted for IFS-137 are
 623 shown in Table 2.

624

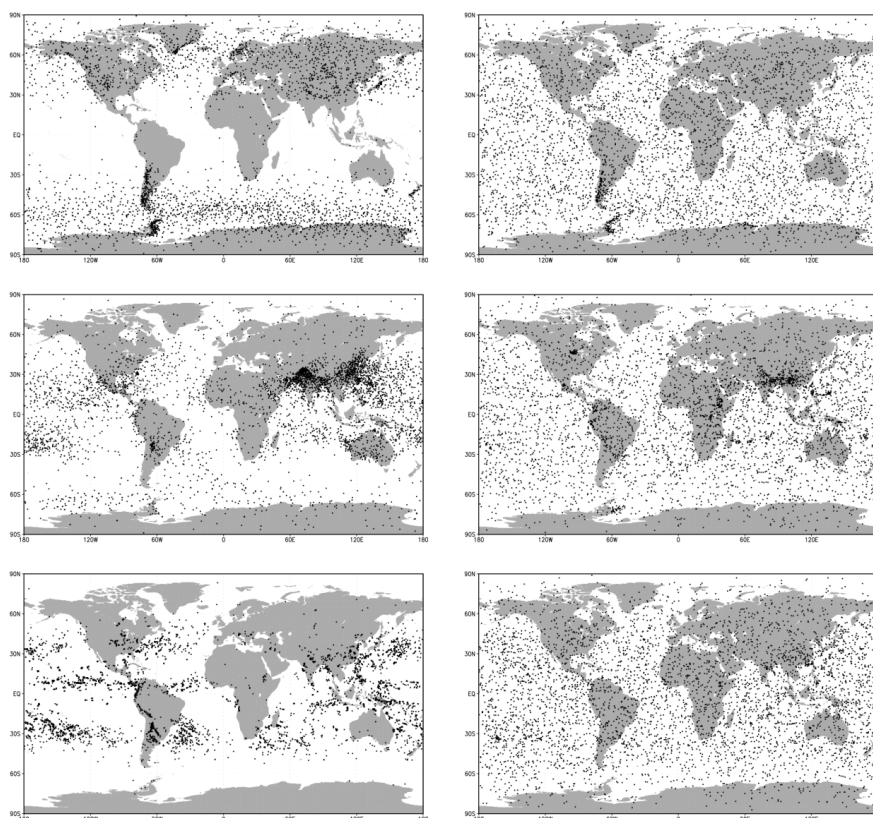
625 **Table 2.** Pressure levels adopted for IFS-137 137 pressure levels (in
 626 hPa).

Level number	pressure hPa								
1	0.02	31	12.8561	61	106.4153	91	424.019	121	934.7666
2	0.031	32	14.2377	62	112.0681	92	441.5395	122	943.1399
3	0.0467	33	15.7162	63	117.9714	93	459.6321	123	950.9082
4	0.0683	34	17.2945	64	124.1337	94	478.3096	124	958.1037
5	0.0975	35	18.9752	65	130.5637	95	497.5845	125	964.7584
6	0.1361	36	20.761	66	137.2703	96	517.4198	126	970.9046
7	0.1861	37	22.6543	67	144.2624	97	537.7195	127	976.5737
8	0.2499	38	24.6577	68	151.5493	98	558.343	128	981.7968
9	0.3299	39	26.7735	69	159.1403	99	579.1926	129	986.6036
10	0.4288	40	29.0039	70	167.045	100	600.1668	130	991.023
11	0.5496	41	31.3512	71	175.2731	101	621.1624	131	995.0824
12	0.6952	42	33.8174	72	183.8344	102	642.0764	132	998.8081
13	0.869	43	36.4047	73	192.7389	103	662.8084	133	1002.225
14	1.0742	44	39.1149	74	201.9969	104	683.262	134	1005.356
15	1.3143	45	41.9493	75	211.6186	105	703.3467	135	1008.224
16	1.5928	46	44.9082	76	221.6146	106	722.9795	136	1010.849
17	1.9134	47	47.9915	77	231.9954	107	742.0855	137	1013.25
18	2.2797	48	51.199	78	242.7719	108	760.5996		
19	2.6954	49	54.5299	79	253.9549	109	778.4661		
20	3.1642	50	57.9834	80	265.5556	110	795.6396		
21	3.6898	51	61.5607	81	277.5852	111	812.0847		
22	4.2759	52	65.2695	82	290.0548	112	827.7756		
23	4.9262	53	69.1187	83	302.9762	113	842.6959		



24	5.6441	54	73.1187	84	316.3607	114	856.8376
25	6.4334	55	77.281	85	330.2202	115	870.2004
26	7.2974	56	81.6182	86	344.5663	116	882.791
27	8.2397	57	86.145	87	359.4111	117	894.6222
28	9.2634	58	90.8774	88	374.7666	118	905.7116
29	10.372	59	95.828	89	390.645	119	916.0815
30	11.5685	60	101.0047	90	407.0583	120	925.7571

627 The locations of selected profiles of temperature, specific
628 humidity, and cloud condensate subsets of the IFS-91 and IFS-137
629 databases are plotted on the map in Fig. 8. In the IFS-91 database,
630 the sampling is fully determined by the selection algorithm, which
631 makes the geographical distributions very inhomogeneous. Selected
632 profiles represent those regions where gradients of the sampled
633 variable are the strongest: in the case of temperature, mid- and
634 high-latitudes dominate, while humidity and cloud condensate
635 subsets concentrate at low latitudes. However, the IFS-137 database
636 shows a much more homogeneous spatial distribution in all the
637 sampling subsets, which is a consequence of the randomized
638 selection.
639



640

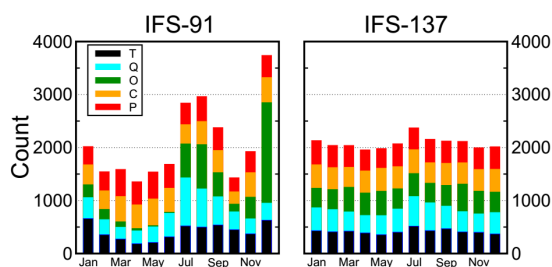
641 **Figure 8.** Locations of selected profiles in the temperature (top),
642 specific humidity (middle), and cloud condensate (bottom), sampled
643 subsets of the IFS-91 (left) and IFS-137 (right) databases (from
644 <https://www.nwpsaf.eu/site/update-137-level-nwp-profile-dataset/> ,
645 2019).

646

647 The temporal distribution of the selected profiles is illustrated in
648 Fig. 9. Again, the lack of randomized selection results in large
649 variations from one month to the next in the case of the IFS-91



650 database (left panel). The different distributions come mainly from
651 variations in the ozone subset (green parts of each column).
652 Dominance of randomly-selected profiles in the IFS-137 database
653 leaves little room for monthly variation in the data count (right
654 panel). Moreover, the IFS-91 database also supports the mode with
655 input parameters, such as detection angle, 2 m temperature, cloud
656 information, and so on. Therefore, it is feasible to use the selected
657 samples in a statistical multiple regression experiment.



658 **Figure 9.** Distribution of profiles within the calendar months in
659 IFS-91 (left) and IFS-137 (right) databases. Different subsets are
660 shown in different colors. Black parts stand for temperature. Blue
661 parts represent specific humidity. Green parts indicate ozone subset.
662 Orange parts stand for cloud condensate. Red parts represent
663 precipitation. (from
664 <https://www.nwpsaf.eu/site/update-137-level-nwp-profile-dataset/>,
665 2019).

666

667 4.2 Experimental scheme



668 In order to verify the retrieval effectiveness of ICS, 5000
669 temperature profiles provided by the IFS-137 were used for
670 statistical inversion comparison experiments. The steps are as
671 follows:

672 (1) 5000 profiles and their corresponding surface factors,
673 including surface air pressure, surface temperature, 2 m temperature,
674 2 m specific humidity, 10 m wind speed, etc. are put into the RTTOV
675 mode. Then, the AIRS observation brightness temperature is
676 obtained.

677 (2) The retrieval of temperature is carried out in accordance with
678 Eq. (23). The 5000 profiles are divided into two groups. The first
679 group of 2500 profiles is used to obtain the regression coefficient,
680 and the second group of 2500 is used to test the result.

681 (3) Verification of the results. The test is carried out based on the
682 standard deviation between the retrieval value and the true value.

683

684 **4.3 Results and Discussion**

685 For the statistical inversion comparison experiments, the standard
686 deviation of temperature retrieval is shown in Fig. 10. First, because
687 PCS does not take channel sensitivity as a function of height into
688 consideration, the retrieval result of PCS is inferior to that of ICS.
689 Second, by comparing the results of ICS and NCS we found that



690 below 100 hPa, since the method used in this paper considers near
691 ground to be less of an influencing factor, the channel combination
692 of ICS is slightly inferior to that of NCS, but the difference is small.

693 From 100 hPa to 10 hPa, the retrieval temperature of ICS in this
694 paper is consistent with that of NCS, slightly better than the channel
695 selected for NCS. From 10 hPa to 0.02 hPa, near the space layer, the
696 retrieval temperature of ICS is obviously better than that of NCS. In
697 terms of the standard deviation, the channel combination of ICS is
698 slightly better than that of PCS from 100 hPa to 10 hPa. From 10
699 hPa to 0.02 hPa, the standard deviation of ICS is lower than that of
700 NCS at about 1 K, meaning that the retrieval result of ICS is better
701 than that of NCS.

702 In order to further illustrate the effectiveness of ICS, the mean
703 improvement value of the ICS and its percentages compared with the
704 PCS and NCS in different height are shown in Table 3. Because PCS
705 does not take channel sensitivity as a function of height into
706 consideration, the retrieval result of PCS is inferior to that of ICS. In
707 general, the accuracy of the retrieval temperature of ICS is improved.
708 Especially, from 100 hPa to 0.01 hPa, the mean value of ICS is
709 evidently improved by more than 0.5 K which means the accuracy
710 can be improved by more than 11%. By comparing the results of ICS
711 and NCS we found that below 100 hPa, since the method used in this



712 paper considers near ground to be less of an influencing factor, the
713 channel combination of ICS is slightly inferior to that of NCS, but
714 the difference is small. From 100 hPa to 0.01 hPa, the mean value of
715 ICS is improved by more than 0.36 K which means the accuracy can
716 be improved by more than 9.6%.

717

718 **Table 3.** The mean improvement value of the ICS and its
719 percentages compared with the PCS and NCS in different height.

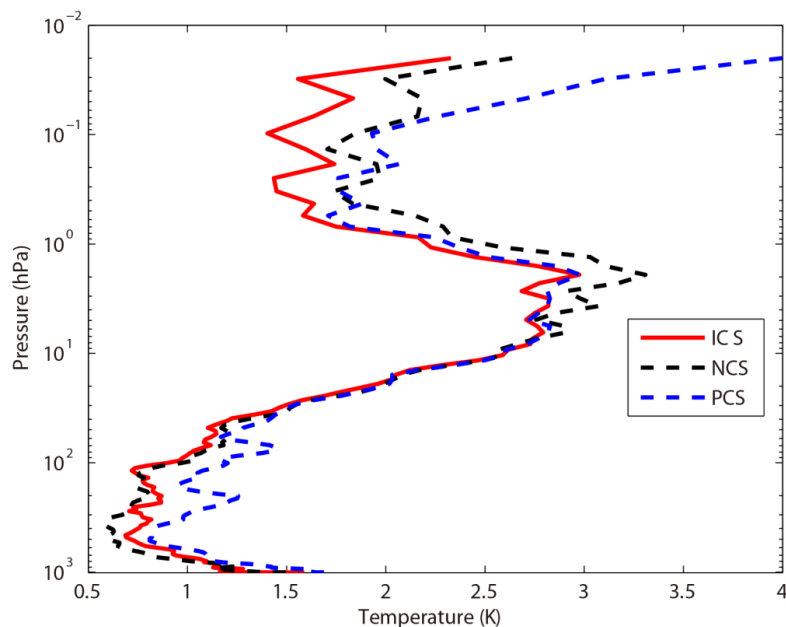
Pressure	Improved mean value /Percentage compared with PCS	Improved value /Percentage compared with NCS
hPa	K/%	K/%
surface-100hPa	0.24/10.77%	-0.04/-3.27%
100hPa-10hPa	0.15/5.08%	0.06/2.4%
10hPa-1hPa	0.04/0.64%	0.17/2.99%
1hPa-0.01hPa	0.52/11.92%	0.36/9.57%

720

721 This is because, as shown in Fig. 4: (1) Near space (20–100 km) is
722 less affected by the ground surface, so the retrieval result of PCS is
723 better than that of NCS. (2) Due to the method selected in this paper,
724 there are more channels at 4.2 μm for N_2O and 4.3 μm for CO_2
725 absorption bands, and the channel combination of PCS is superior to
726 that of NCS for atmospheric temperature detection in the high
727 temperature zone. Moreover, ICS takes channel sensitivity as a
728 function of height into consideration, so its retrieval result is
729 impressive.



730



731

732 **Figure 10.** The temperature profile standard deviation of statistical
733 inversion comparison experiments. Red line indicates the result of
734 ICS. Black dotted line stands for the result of NCS. Blue dotted line
735 represents the result of PCS.

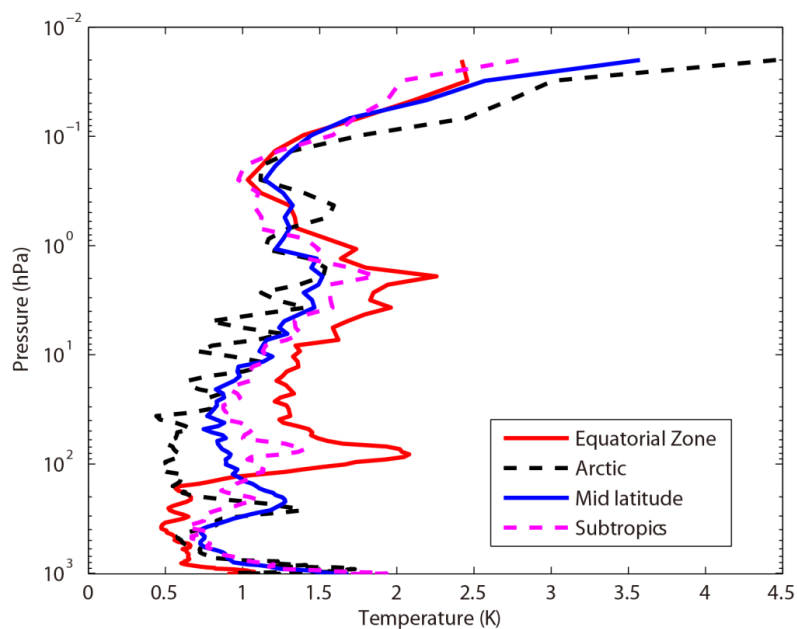
736

737 **5 Statistical inversion comparison experiments in four typical** 738 **regions**

739 The accuracy of the retrieval temperature varies from place to place
740 and changes with weather conditions. Therefore, in order to further
741 compare the inversion accuracy under different atmospheric
742 conditions, the atmospheric profile is from the IFS-137 database



743 introduced in Sect. 4, and divides it into four regions: equatorial
744 zone, subtropical region, mid-latitude region and Arctic. These
745 regions' profiles can represent the global typical atmospheric
746 temperature profiles. The average temperature profiles in these four
747 regions are shown in Fig. 11. The retrieval temperature varies from
748 place to place and changes with weather conditions
749



750
751 **Figure 11.** The average temperature profiles in four typical regions.
752 Red line indicates the equatorial zone. Pink dotted line stands for the
753 subtropics. Blue dotted line represents the mid-latitude region. Black
754 dotted line stands for the Arctic.
755



756

757 **5.1 Experimental scheme**

758 In order to further illustrate the different accuracy of the retrieval
759 temperature using our improved channel selection method under
760 different atmospheric conditions, the profiles in four typical regions
761 were used for statistical inversion comparison experiments. The
762 experimental steps are as follows:

763 (1) 2500 profiles in Sect. 4 are used to work out the regression
764 coefficient.

765 (2) The atmospheric profiles of the four typical regions: equatorial
766 zone, subtropical region, mid-latitude region and Arctic are used for
767 statistical inversion comparison experiments and test the result.(3)
768 Verification of the results. The test is carried out based on the
769 standard deviation between the retrieval value and the true value.

770

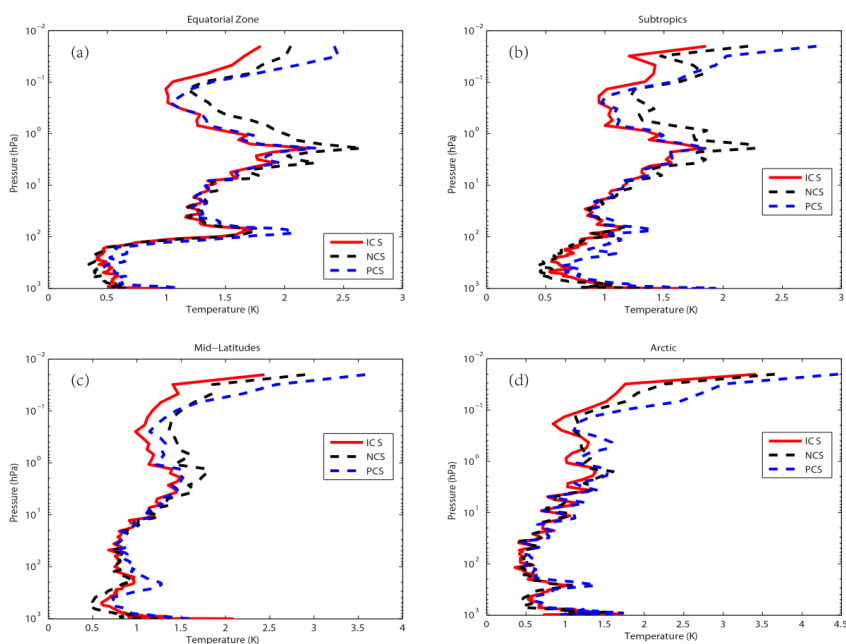
771 **5.2 Results and Discussion**

772 Using statistical inversion comparison experiments in four typical
773 regions, the standard deviation of temperature retrieval is shown in
774 Fig. 12. Generally, the retrieval temperature by ICS is greatly
775 superior to that of NCS and PCS. In particular, above 1 hPa (the near
776 space layer), the standard deviation of atmospheric temperature can
777 be optimized to 1 K with PCS and NCS. Thus, ICS shows a great



778 improvement. The results were consistent with Sect. 4.

779



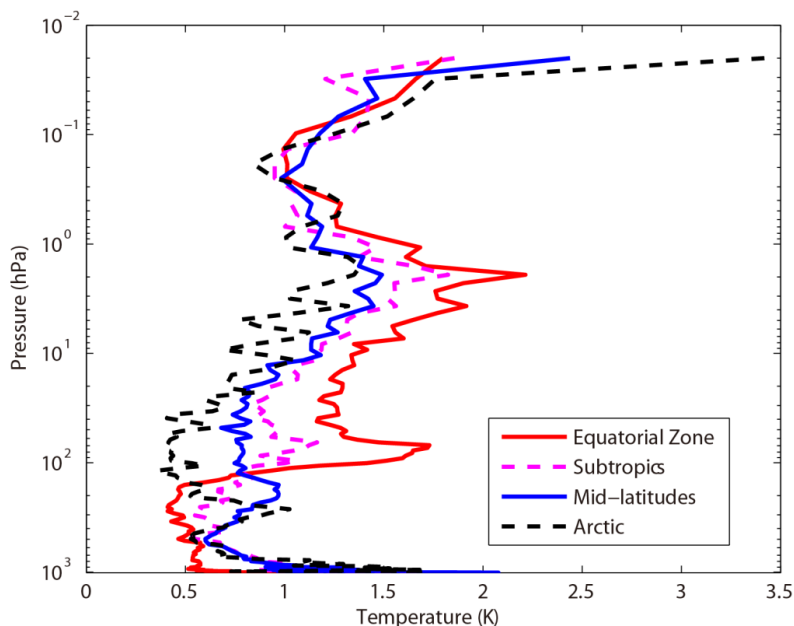
780

781 **Figure 12.** The temperature profile standard deviation of statistical
782 inversion comparison experiments in four typical regions. Red line
783 indicates the result of ICS. Black dotted line stands for the result of
784 NCS. Blue dotted line represents the result of PCS. (a) Equatorial
785 zone. (b) Subtropics. (c) Mid-latitudes. (b) Arctic.

786

787 In order to further compare the regional differences of inversion
788 accuracy, the temperature standard deviation of ICS in four typical
789 regions are compared in Fig. 13.

790



791

792 **Figure 13.** The temperature standard deviation of ICS in four typical
793 regions. Red line indicates the result of equatorial zone. Pink dotted
794 line represents the result of Subtropics. Blue line represents the
795 result of Mid-latitudes. Black dotted line stands for the result of
796 Arctic.

797

798 As can be seen from Fig. 13, the temperature standard deviations
799 of the ICS in the four typical regions are large. Below 100 hPa, due
800 to the high temperature in the equatorial zone, the channel
801 combination of ICS is superior to that of PCS and NCS for
802 atmospheric temperature detection in the high temperature zone. The
803 standard deviation is 0.5K. Due to the method selected in this paper



804 there are more channels at 4.2 μm for N_2O and 4.3 μm for CO_2
805 absorption bands which has been previously described in Sect. 3.
806 Near the tropopause, the standard deviation of the equatorial zone
807 increases sharply. It is also due to the sharp drops in temperature.
808 However, the standard deviation of the Arctic is still around 0.5K.
809 From 100hPa to 1hPa, the standard deviation of ICS is 0.5 K to 2K.
810 With the increase of latitude, the effectiveness considerably
811 increases. According to Fig. 12, ICS takes channel sensitivity as a
812 function of height into consideration, so its retrieval result is
813 impressive.

814 In order to further illustrate the effectiveness of ICS, the mean
815 improvement value of the ICS and its percentages compared with the
816 PCS and NCS in different height of four typical regions are shown in
817 Table 4 to Table 7.

818

819 **Table 4.** The mean improvement value of the ICS and its
820 percentages compared with the PCS and NCS in different height in
821 equatorial zone.

Pressure	Improved mean value /Percentage compared with PCS	Improved value /Percentage compared with NCS
hPa	K/%	K/%
surface-100hPa	0.18/12.25%	-0.06/-5.61%
100hPa-10hPa	0.13/4.23%	0.04/1.28%
10hPa-1hPa	0.03/0.09%	0.24/6.24%



1hPa-0.01hPa 0.24/7.41% 0.33/11.22%

822

823 **Table 5.** The mean improvement value of the ICS and its
 824 percentages compared with the PCS and NCS in different height in
 825 subtropics.

Pressure	Improved mean value	Improved value
	/Percentage compared with PCS	/Percentage compared with NCS
hPa	K/%	K/%
surface-100hPa	0.26/12.49%	-0.08/-5.94%
100hPa-10hPa	0.08/3.55%	0.02/1.28%
10hPa-1hPa	0.02/0.56%	0.2/5.94%
1hPa-0.01hPa	0.25/7.73%	0.34/12.51%

826

827 **Table 6.** The mean improvement value of the ICS and its
 828 percentages compared with the PCS and NCS in different height in
 829 mid-latitudes.

Pressure	Improved mean value	Improved value
	/Percentage compared with PCS	/Percentage compared with NCS
hPa	K/%	K/%
surface-100hPa	0.18/9.23%	-0.13/-7.41%
100hPa-10hPa	0.06/3.68%	0.03/1.84%
10hPa-1hPa	0.03/1.03%	0.18/6.01%
1hPa-0.01hPa	0.36/10.64%	0.36/12.71%

830

831 **Table 7.** The mean improvement value of the ICS and its
 832 percentages compared with the PCS and NCS in different height in
 833 Arctic.



Pressure	Improved mean value /Percentage compared with PCS	Improved value /Percentage compared with NCS
hPa	K/%	K/%
surface-100hPa	0.12/6.52%	-0.05/-3.47%
100hPa-10hPa	0.08/6.59%	0.02/1.97%
10hPa-1hPa	0.09/3.64%	0.06/2.5%
1hPa-0.01hPa	0.49/13.72%	0.18/6.47%

834

835 Although the improvements of ICS in the four typical regions are
836 different, in general, the accuracy of the retrieval temperature of ICS
837 is improved. Because PCS does not take channel sensitivity as a
838 function of height into consideration, the retrieval result of PCS is
839 inferior to that of ICS. In general, the accuracy of the retrieval
840 temperature of ICS is improved. Especially, from 100 hPa to 0.01
841 hPa, the accuracy of ICS can be improved by 7% to 13%. By
842 comparing the results of ICS and NCS we found that below 100 hPa,
843 since the method used in this paper considers near ground to be less
844 of an influencing factor, the channel combination of ICS is slightly
845 inferior to that of NCS, but the difference is small. From 100 hPa to
846 0.01 hPa, the accuracy of ICS can be improved by 7% to 13%.

847

848 **6. Conclusions and discussion**

849 **6.1 Conclusions**

850 An improved channel selection method is proposed, based on



851 information content in this paper. A robust channel selection scheme
852 and method are proposed, and a series of channel selection
853 comparison experiments are conducted. The results are as follows:
854 (1) Since ICS takes channel sensitivity as a function of height into
855 consideration, the ARI of PCS only tends to be 0.38 and is not
856 convergent. However, as the 100th iteration is approached, the ARI of
857 ICS tends to be stable, reaching 0.54, while the distribution of the
858 temperature weight function is more continuous and closer to that of
859 the actual atmosphere. Thus, in terms of the ARI, convergence, and
860 the distribution of the temperature weight function, ICS is superior
861 to PCS.

862 (2) Statistical inversion comparison experiments show that the
863 retrieval temperature of ICS in this paper is consistent with that of
864 NCS. In particular, from 10 hPa to 0.02 hPa (the near space layer),
865 the retrieval temperature of ICS is obviously better than that of NCS
866 at about 1 K. In general, the accuracy of the retrieval temperature of
867 ICS is improved. Especially, from 100 hPa to 0.01 hPa, the accuracy
868 of ICS can be improved by more than 11%. The reason is that near
869 space (20–100 km) is less affected by the ground surface, so the
870 retrieval result of ICS is better than that of NCS. Additionally, due to
871 the method selected in this paper there are more channels at 4.2 μm
872 for the N₂O and 4.3 μm for the CO₂ absorption bands; the channel



873 combination of ICS is superior to that of NCS for atmospheric
874 temperature detection in the high temperature zone.

875 (3) Statistical inversion comparison experiments in four typical
876 regions indicate that ICS in this paper is significantly better than
877 NCS and PCS in different regions and shows latitudinal variations.
878 Especially, from 100 hPa to 0.01 hPa, the accuracy of ICS can be
879 improved by 7% to 13%, which means the ICS method selected in
880 this paper is feasible and shows great promise for applications.

881

882 **6.2 Discussion**

883 In recent years, the atmospheric layer in the altitude range of about
884 20–100 km has been named “the near space layer” by aeronautical
885 and astronomical communities. It is between the space-based satellite
886 platform and the aerospace vehicle platform, which is the transition
887 zone between aviation and aerospace. Its unique resource has
888 attracted a lot of attention from many countries. Research and
889 exploration, therefore, on and of the near space layer are of great
890 importance. A new channel selection scheme and method for
891 hyperspectral atmospheric infrared sounder AIRS data based on
892 layering are proposed. The retrieval results of ICS concerning the
893 near space atmosphere are particularly good. Thus, ICS aims to
894 provide a new and an effective channel selection method for the



895 study of the near space atmosphere using the hyperspectral
896 atmospheric infrared sounder.

897

898 *Data availability.* The data used in this paper are available from the
899 corresponding author upon request.

900

901 *Author contributions.* ZS contributed the central idea. SC, ZS and
902 HD conceived the method, developed the retrieval algorithm and
903 discussed the results. SC analyzed the data, prepared the figures and
904 wrote the paper. WG contributed to refining the ideas, carrying out
905 additional analyses. All co-authors reviewed the paper.

906

907 *Competing interests.* The authors declare that they have no conflict
908 of interest.

909

910 *Acknowledgements.* The study was supported by the National
911 Natural Science Foundation of China (Grant no. 41875045). The
912 study was also partly supported by the National Key Research
913 Program of China: Development of high-resolution data assimilation
914 technology and atmospheric reanalysis data set in East Asia
915 (Research on remote sensing telemetry data assimilation technology,
916 Grant no. 2017YFC1501802).



917

918 **References**

919 Aires, F., Schmitt, M., Chedin, A., and Scott, N.: The “weight
920 smoothing” regularization of MLP for Jacobian stabilization,
921 IEEE. T. Neural. Networks., 10, 1502-1510,
922 <https://doi.org/10.1109/72.809096>, 1999.

923 Aires, F., Chédin, Alain., Scott, N. A., and Rossow, W. B.: A
924 regularized neural net approach for retrieval of atmospheric and
925 surface temperatures with the IASI instrument, J. Appl. Meteorol.,
926 41,144-159,
927 [https://doi.org/10.1175/1520-0450\(2002\)041<0144:ARNNAF>2.0](https://doi.org/10.1175/1520-0450(2002)041<0144:ARNNAF>2.0)
928 .CO;2, 2002.

929 Aumann, H. H.: Atmospheric infrared sounder on the earth
930 observing system, Optl. Engr., 33, 776-784,
931 <https://doi.org/10.1117/12.159325>, 1994.

932 Aumann, H. H., Chahine, M. T., Gautier, C., and Goldberg, M.:
933 AIRS/AMSU/HSB on the Aqua mission: design, science objective,
934 data products, and processing systems, IEEE. Trans. GRS.,
935 41,253-264, <http://dx.doi.org/10.1109/TGRS.2002.808356>, 2003.

936 Chahine, M. I.: A general relaxation method for inverse solution of
937 the full radiative transfer equation, J. Atmos. Sci., 29, 741-747,
938 [https://doi.org/10.1175/1520-0469\(1972\)029<0741:AGRMFI>2.0](https://doi.org/10.1175/1520-0469(1972)029<0741:AGRMFI>2.0).



- 939 CO₂, 1972.
- 940 Chang, K. W, L'Ecuyer, T. S., Kahn, B. H., and Natraj, V.:
941 Information content of visible and midinfrared radiances for
942 retrieving tropical ice cloud properties, *J. Geophys. Res.*, 122,
943 <https://doi.org/10.1002/2016JD026357>, 2017.
- 944 Chedin, A., Scott, N. A., Wahiche, C., and Moulinier, P.: The
945 improved initialization inversion method: a high resolution
946 physical method for temperature retrievals from satellites of the
947 tiros-n series, *J. Appl. Meteor.*, 24, 128-143,
948 [https://doi.org/10.1175/1520-0450\(1985\)024<0128:TIHIMA>2.0.CO;2](https://doi.org/10.1175/1520-0450(1985)024<0128:TIHIMA>2.0.CO;2), 1985.
- 949
- 950 Cyril, C., Alain, C., and Scott, N. A.: Airs channel selection for CO₂
951 and other trace-gas retrievals, *Q. J. Roy. Meteor. Soc.*, 129,
952 2719-2740, <https://doi.org/10.1256/qj.02.180>, 2003.
- 953 Du, H. D., Huang, S. X., and Shi, H. Q.: Method and experiment of
954 channel selection for high spectral resolution data, *Acta. Physica.*
955 *Sinica.*, 57, 7685-7692, 2008 .
- 956 Eyre, J. R., Andersson E., and McNally, A. P.: Direct use of
957 satellite sounding radiances in numerical weather prediction, *High*
958 *Spectral Resolution Infrared Remote Sensing for Earth's Weather*
959 *and Climate Studies*, Springer, Berlin, Heidelberg,
960 https://doi.org/10.1007/978-3-642-84599-4_25, 1993.



- 961 Fang, Z. Y.: The evolution of meteorological satellites and the
962 insight from it, *Adv. Meteorol. Sci. Technol.*, 4, 27-34,
963 <https://doi.org/10.3969/j.issn.2095-1973.2014.06.003>, 2014.
- 964 Gong, J., Wu, D. L., and Eckermann, S. D.: Gravity wave variances
965 and propagation derived from AIRS radiances, *Atmos. Chem.*
966 *Phys.*, 11, 11691-11738,
967 <https://doi.org/10.5194/acp-12-1701-2012>, 2011.
- 968 He, M. Y., Du, H. D., Long, Z. Y., and Huang, S. X.: Selection of
969 regularization parameters using an atmospheric retrievable index
970 in a retrieval of atmospheric profile, *Acta. Physica Sinica.*, 61,
971 024205-160, 2012.
- 972 Hoffmann, L. and Alexander, M. J.: Retrieval of stratospheric
973 temperatures from atmospheric infrared sounder radiance
974 measurements for gravity wave studies, *J. Geophys. Res. Atm.*,
975 114, <https://doi.org/10.1029/2008JD011241>, 2009.
- 976 Huang, H. L., Li, J., Baggett, K., Smith, W. L., and Guan, L.:
977 Evaluation of cloud-cleared radiances for numerical weather
978 prediction and cloud-contaminated sounding applications,
979 *Atmospheric and Environmental Remote Sensing Data Processing*
980 *and Utilization: Numerical Atmospheric Prediction and*
981 *Environmental Monitoring*, I. S. O. Photonics.,
982 <https://doi.org/10.1117/12.613027>, 2005.



- 983 Kuai, L., Natraj, V., Shia, R. L., Miller, C., and Yung, Y. L.: Channel
984 selection using information content analysis: a case study of CO₂
985 retrieval from near infrared measurements. *J. Q. S. Radiative*.
986 *Transfer.*, 111, 1296-1304,
987 <https://doi.org/10.1016/j.jqsrt.2010.02.011>, 2010.
- 988 Li, J., Wolf, W. W., Menzel, W. P., Paul, Menzel. W., Zhang, W. J.,
989 Huang, H. L., and Achtor, T. H.: Global soundings of the
990 atmosphere from ATOVS measurements: the algorithm and
991 validation, *J. Appl. Meteor.*, 39, 1248-1268,
992 [https://doi.org/10.1175/1520-0450\(2000\)039<1248:GSOTAF>2.0](https://doi.org/10.1175/1520-0450(2000)039<1248:GSOTAF>2.0).
993 CO₂, 2000.
- 994 Li, J., Liu, C. Y., Huang, H. L., Schmit, T. J., Wu, X., Menzel, W. P.,
995 and Gurka, J. J.: Optimal cloud-clearing for AIRS radiances using
996 MODIS, *IEEE. Trans. GRS.*, 43, 1266-1278, [http://dx.doi.org/](http://dx.doi.org/10.1109/tgrs.2005.847795)
997 [10.1109/tgrs.2005.847795](http://dx.doi.org/10.1109/tgrs.2005.847795), 2005.
- 998 Liu, Z. Q.: A regional ATOVS radiance-bias correction scheme for
999 radiance assimilation, *Acta. Meteorologica. Sinica.*, 65, 113-123,
1000 2007.
- 1001 Lupu, C., Gauthier, P., and Laroche, Stéphane.: Assessment of the
1002 impact of observations on analyses derived from observing system
1003 experiments, *Mon. Weather. Rev.*, 140, 245-257,
1004 <https://doi.org/10.1175/MWR-D-10-05010.1>, 2012.



- 1005 Menke, W.: Geophysical Data Analysis: Discrete Inverse Theory,
1006 Acad. Press., Columbia University, New York,
1007 <https://doi.org/10.1016/B978-0-12-397160-9.00019-9>, 1984.
- 1008 Prunet, P., Thépaut J. N., and Cass, V.: The information content of
1009 clear sky IASI radiances and their potential for numerical weather
1010 prediction, *Q. J. Roy. Meteor. Soc.*, 124, 211-241,
1011 <https://doi.org/10.1002/qj.49712454510>, 2010.
- 1012 Xu, Q.: Measuring information content from observations for data
1013 assimilation: relative entropy versus shannon entropy difference,
1014 *Tellus. A.*, 59, 198-209,
1015 <https://doi.org/10.1111/j.1600-0870.2006.00222.x>, 2007.
- 1016 Rabier, F., Fourrié, N., and Chafäi, D.: Channel selection methods
1017 for infrared atmospheric sounding interferometer radiances, *Q. J.*
1018 *Roy. Meteor. Soc.*, 128, 1011-1027,
1019 <https://doi.org/10.1256/0035900021643638>, 2010.
- 1020 Richardson, M. and Stephens, G. L.: Information content of oco-2
1021 oxygen a-band channels for retrieving marine liquid cloud
1022 properties, *Atmospheric Measurement Techniques*, 11, 1-19,
1023 <https://doi.org/10.5194/amt-11-1515-2018>, 2018.
- 1024 Rodgers, C. D.: Information content and optimisation of high
1025 spectral resolution remote measurements, *Adv. Spa. Research*, 21,
1026 136-147, [https://doi.org/10.1016/S0273-1177\(97\)00915-0](https://doi.org/10.1016/S0273-1177(97)00915-0), 1996.



- 1027 Rodgers, C. D.: Inverse Methods for Atmospheric Sounding, Inverse
1028 methods for atmospheric sounding, World Scientific,
1029 <https://doi.org/10.1142/3171>, 2000.
- 1030 Smith, W. L., Woolf, H. M., and Revercomb, H. E.: Linear
1031 simultaneous solution for temperature and absorbing constituent
1032 profiles from radiance spectra, *Appl. Optics.*, 30, 1117,
1033 <https://doi.org/10.1364/AO.30.001117>, 1991.
- 1034 Wakita, H., Tokura, Y., Furukawa, F., and Takigawa, M.: Study of
1035 the information content contained in remote sensing data of
1036 atmosphere, *Acta. Physica. Sinica.*, 59, 683-691, 2010.
- 1037 Wang, G., Lu, Q. F., Zhang, J. W., and Wang, H. Y.,.: Study on
1038 method and experiment of hyper-spectral atmospheric infrared
1039 sounder channel selection, *Remote Sensing Technology and
1040 Application.*, 29, 795-802 , 2014.
- 1041 Zhang, J. W., Wang, G., Zhang, H., Huang J., Chen J., and Wu, L. L.:
1042 Experiment on hyper-spectral atmospheric infrared sounder
1043 channel selection based on the cumulative effect coefficient of
1044 principal component, *Journal of Nanjing Institute of meteorology*,
1045 1, 36-42, <http://dx.doi.org/10.3969/j.issn.1674-7097.2011.01.005>,
1046 2011.